1*n* and 2*n* Transfer With the Borromean Nucleus ⁶He Near the Coulomb Barrier

A. Chatterjee,[1,2] A. Navin,[1,*] A. Shrivastava,[2] S. Bhattacharyya,[1] M. Rejmund,[1] N. Keeley,[3,4] V. Nanal,[5] J. Nyberg,[6]
R. G. Pillay,[5] K. Ramachandran,[2] I. Stefan,[1] D. Bazin,[7] D. Beaumel,[8] Y. Blumenfeld,[8] G. de France,[1] D. Gupta,[8]
M. Labiche,[9] A. Lemasson,[1] R. Lemmon,[9] R. Raabe,[1] J. A. Scarpaci,[8] C. Simenel,[3] and C. Timis[10]

[1]*GANIL, CEA/DSM–CNRS/IN2P3, Bd Henri Becquerel, BP 55027, F-14076 Caen Cedex 5, France*
[2]*Nuclear Physics Division, Bhabha Atomic Research Centre, Mumbai 400085, India*
[3]*DSM/IRFU/SPhN, CEA Saclay, F-91191 Gif sur Yvette, France*
[4]*Department of Nuclear Reactions, The Andrzej Sołtan Institute for Nuclear Studies, Hoża 69, PL-00-681 Warsaw, Poland*
[5]*DNAP, Tata Institute of Fundamental Research, Mumbai 400005, India*
[6]*Department of Physics and Astronomy, Uppsala University, Uppsala, Sweden*
[7]*National Superconducting Cyclotron Laboratory, Michigan State University, East Lansing, Michigan, 48824, USA*
[8]*Institut de Physique Nucléaire, IN2P3-CNRS, 91406 Orsay, France*
[9]*CRLC, Daresbury Laboratory, Daresbury, Warrington, WA4 4AD, United Kingdom*
[10]*Department of Physics, University of Surrey, Guildford, GU2 7XH, United Kingdom*

Angular distributions for 1*n* and 2*n* transfer are reported for the ⁶He + ⁶⁵Cu system at $E_{lab} =$ 22.6 MeV. For the first time, triple coincidences between α particles, neutrons, and characteristic γ rays from the targetlike residues were used to separate the contributions arising from 1*n* and 2*n* transfer. The differential cross sections for these channels, elastic scattering, and fusion were analyzed using a coupled reaction channels approach. The large measured ratio of the 2*n*-to- 1*n* cross section and the strong influence of 2*n* transfer on other channels indicate that the dineutron configuration of ⁶He plays a dominant role in the reaction mechanism.

Reactions near the Coulomb barrier have been shown to be an ideal tool to study the effect of multidimensional tunneling and obtain information about the structure of the interacting nuclei [1]. New features arising from the weak binding in nuclei far from stability in reactions near the Coulomb barrier have been recently discussed [2]. Neutron-rich nuclei near the drip line, especially Borromean nuclei, offer a unique environment to study neutron correlations at low densities, which are necessary inputs for nuclear structure models and the study of neutron stars. Theoretical analyses suggest that at low neutron density strong spatial dineutron correlations are expected [3,4]. Such correlations have been theoretically studied in two-neutron Borromean nuclei like ⁶He and ¹¹Li [5]. The structure of the lightest two-neutron halo nucleus, ⁶He, with an inert α core and known α-*n* interaction has been investigated via a variety of techniques [6–9], mainly at energies well above the Coulomb barrier.

The 2*n*-to- 1*n* transfer cross section ratio can provide information about the structural correlation of neutrons in ⁶He. The cigar shape, where the two neutrons lie on opposite sides of the α particle, should preferentially populate ⁵He by 1*n* transfer while the dineutron configuration should be responsible mainly for 2*n* transfer [10]. The recently reported charge radii of ⁶,⁸He provide an independent method of studying correlations in these Borromean nuclei [11]. Michel *et al.* have investigated the Wigner threshold law in weakly bound nuclei using the Gamow shell model [12], showing the influence of the

Wigner cusp on the spectroscopic factors. Thus, the study of transfer angular distributions with Borromean nuclei is of interest in the context of this general phenomenon observed in various fields of physics [13].

Measurements of α-*n* coincidences in the ⁶He + ²⁰⁹Bi system at an energy of 22 MeV showed the relative dominance of the 2*n* channel [14,15]. Reactions on medium-mass targets are experimentally more challenging and are also controversial with respect to the influence of weak binding on the fusion process [16]. Theoretical treatment of reactions involving Borromean projectiles, especially at near-barrier energies, is a complex problem as calculations have to include the unbound spectrum of a four-body system. However, state-of-the-art continuum discretized coupled-channel calculations taking into account the three-body nature of ⁶He [17,18] or its simplification as a $2n + \alpha$ cluster [19] have been performed. These calculations can presently compute only elastic scattering and breakup; a theoretical formalism able to describe simultaneously elastic scattering, transfer, and breakup is desirable but not yet available.

With the motivation of understanding the Borromean structure and its influence on reactions around the Coulomb barrier, we report a novel triple coincidence measurement of angular distributions of transfer channels with an ISOL beam. A first theoretical attempt, for Borromean nuclei, towards understanding the importance of coupling to transfer channels for elastic scattering and fusion is also presented.

An intense ($\sim 4 \times 10^7$ pps) ^{6}He beam at an energy of
22.6 MeV was obtained from the ISOL facility SPIRAL at
GANIL. The target was a 2.6 mg/cm^2 thick self-
supporting ^{65}Cu foil, isotopically enriched to 99.7%.
Beam intensities were measured with a high stability cur-
rent amplifier connected to a Faraday cup. The detection
setup [Fig. 1(a)] consisted of an annular Si telescope, the
EXOGAM γ array [20] with 11 Compton-suppressed clo-
vers, and a neutron array of 45 liquid scintillator elements
[21].

Charged particles were detected and identified in an
annular Si telescope comprising ΔE ($\sim 50 \mu$m) and E
($\sim 500 \mu$m) elements with active inner and outer diameters
of 22 and 70 mm covering an angular range of $\sim 25°$–$60°$
at 2.5 cm from the target. The angular resolution was
$\simeq 1.7°$. The solid angles of each ring-sector combination
were determined both by simulations and comparison with
elastic scattering measurements on a Au target. The energy
resolution for elastically scattered particles was
$\simeq 300$ keV. The neutron wall consisted of 45 hexagonal
detectors at 55 cm from the target, covering $\simeq 18\%$ of 4π
[21]. The time of flight (TOF) was obtained with respect to
the E detector of the annular telescope with a resolution of
$\simeq 3$ ns (corresponding to an energy resolution of 270 keV at
$E_n = 1.5$ MeV). Neutrons were separated from γ rays by
two-dimensional gates in the TOF versus pulse-shape dis-
crimination plot and detected at mean angles of 19°, 30°,
35°, 47°, and 57° with an angular resolution of $\pm 6.5°$.
Small corrections for cross talk between the neutron de-
tectors were included [22]. Absolute efficiencies of the
neutron detectors as a function of energy were determined
from a comparison of the measured neutron spectra from a
^{252}Cf source placed at the target position and the known
multiplicity and spectral shape [23]. The measured effi-
ciencies compared well with Monte Carlo simulations of
the neutron array [22]. Eleven Compton-suppressed clover
detectors at 14.7 cm from the target were used to select the
residual nuclei by a measurement of their characteristic
γ rays. Cross sections for the evaporation residue channels
were obtained from characteristic γ ray yields, following
the method of Ref. [16]. The total fusion cross section was
obtained from the sum of the measured evaporation residue
cross sections. Statistical model calculations using the
code CASCADE [24] showed good agreement for all resi-
dues except ^{66}Cu. The yield of ^{66}Cu from fusion evapora-
tion is negligible ($\approx 5\%$); it is produced mainly by 1n and
2n transfer (see also [16]).

Figure 1(b) gives a schematic of the reaction mecha-
nism, indicating that due to the Borromean nature of ^{6}He
the final state is similar in both 1n and 2n transfer. In both
cases we have a neutron, an α particle, and γ rays from the
excited ^{66}Cu residue. Transfer is a selective process, peak-
ing for a narrow window of matching conditions in the
angular and linear momenta of the particles. In the present
case, 2n transfer leads to the formation of ^{67}Cu with an
excitation energy sufficient to evaporate one neutron (iso-
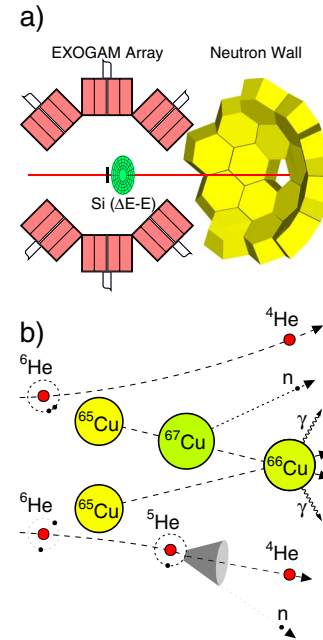tropically), while 1n transfer leads to states in ^{66}Cu which

FIG. 1 (color online).   Schematic of (a) the experimental setup.
(b) Reaction mechanism for 2n and 1n transfer

decay by γ emission. Hence there is a kinematic correla-
tion (conditions on energies and emission angles) between
α particles and neutrons for 1n transfer but not for 2n
transfer. Triple coincidences between n, α, and γ rays from
the excited ^{66}Cu residue were used to deconvolute the 1n
and 2n transfer contributions and eliminate projectile
breakup. Extraction of the transfer cross section was as
follows. Events with conditions for neutron, α particle, and
γ transitions in ^{66}Cu were first selected. These were then
used to obtain the angles and energies of the selected
neutrons and α particles and their relative angles $\theta_{n\alpha}$ and
energies $E_{n\alpha}$. Population of the $3/2^-$ ground state of ^{5}He
was verified from the measured correlation between $\theta_{n\alpha}$
and $E_{n\alpha}$. For 1n transfer, neutrons and α particles are
emitted by the breakup of ^{5}He in this state. Reaction
kinematics restricts $\theta_{n\alpha}$ to a maximum value (θ_0) of 31°
for these events. Such a directional correlation is absent in
the case of 2n transfer where the neutron arises by evapo-
ration from excited ^{67}Cu nuclei [see Fig. 1(b)]. Thus the
region $\theta_{n\alpha} > \theta_0$ consists of events arising from 2n transfer,
and the corresponding differential cross sections were
obtained by restricting to events in this region. The region
$\theta_{n\alpha} < \theta_0$ contains contributions from both 2n and 1n trans-
fer. Figure 2 shows the sum of the added-back γ-ray
spectrum in coincidence with α particles and neutrons
for $\theta_{n\alpha} > \theta_0$. Prominent transitions in ^{66}Cu and those in
^{65}Cu (arising from the α-2n fusion-evaporation channel)
are indicated. The inset shows the division of the kinematic
region in a two-dimensional plot of Δx versus Δy, where
Δx and Δy are the differences in position of the detected α
particle and neutron at the plane of the Si detector. The
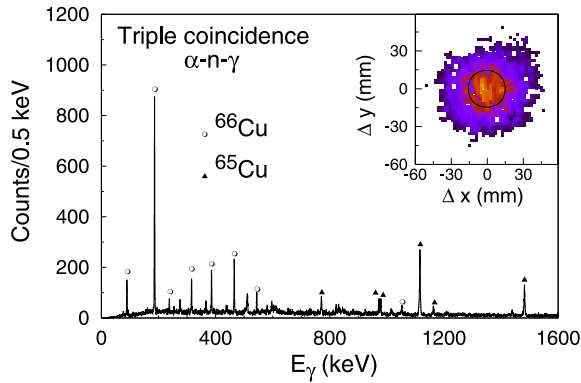central region (marked by a circle in the inset) represents

FIG. 2 (color online). γ spectrum in coincidence with α particles and neutrons obtained by selecting events outside the region marked in the inset (see text). The inset shows a 2D plot of the difference in positions of the detected α particle and neutron at the plane of the Si detector.

the 31° cone. Differential cross sections for $1n$ transfer were obtained by subtracting the $2n$ transfer contribution obtained from the yields outside the cone (scaled with the appropriate solid angles) from the total yields in this region. The emission angle of ^{5}He was approximated as the measured θ_α. The fraction of the solid angle of the neutron wall corresponding to the two regions, inside and outside the cone, was obtained from simulations.

Absolute cross sections were obtained from the known efficiencies, target thickness, and integrated beam intensity. Angular distributions for $1n$ and $2n$ transfer are plotted in Fig. 3(a); only statistical errors are shown, ranging from 2%–3% and 15%–20% for the $2n$ and the $1n$ trans-
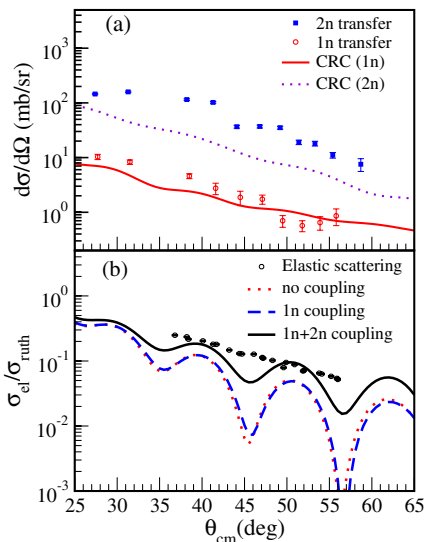

FIG. 3 (color online).   Angular distributions for ^{6}He + ^{65}Cu. (a) $1n$ and $2n$ transfer. Calculations for $1n$ and $2n$ transfer are shown. (b) Elastic scattering. Calculations with no coupling (dotted curve), $1n$ transfer couplings only (dashed line), and both $1n$ and $2n$ transfer couplings (solid line) are shown.

fer, respectively. For $1n$ transfer $\theta_{^5\mathrm{He}}$ was assumed to be equal to θ_α. The relative insensitivity of the extracted cross sections to the precise value of θ_0 was verified by repeating the analysis with a 5° variation. The elastic scattering angular distribution is shown in Fig. 3(b).

Coupled reaction channel (CRC) calculations [2] were performed using the code FRESCO [25] to understand the angular distributions and the role of channel coupling in the various processes. The full complex remnant term and nonorthogonality correction were included. Coupling to breakup channels was not considered, based on a lower breakup contribution (as compared to transfer) observed in [26] and the reduced importance of Coulomb breakup for this lower Z target. Entrance and exit channel potentials consisted of double-folded real and interior Woods-Saxon imaginary parts. The Michigan three-range Yukawa (M3Y) effective interaction [27] and ^{6}He and ^{5}He matter densities from Refs. [28,29], respectively, were used to calculate the real potential. The Woods-Saxon potential parameters were $W = 50$ MeV, $R = 1.0 \times (A_p^{1/3} + A_t^{1/3})$ fm, $a = 0.3$ fm.

The positive Q value of the ^{65}Cu(^{6}He, ^{5}He)^{66}Cu reaction favors population of relatively high-lying states. However, the $(2J + 1)S$ values derived from an analysis of the ^{65}Cu(d, p) reaction show a rather rapid decrease with increasing excitation energy (below ~ 3 MeV) [30]. Thus, a limited number of states in ^{66}Cu were included. Configurations, spectroscopic factors, and $n + {}^{65}$Cu potentials were from Refs. [30,31]. Transfer to the $3/2^-$ resonance of ^{5}He only was included, with spectroscopic factor from Ref. [32] and Woods-Saxon $n + {}^5$He potential with radius parameter $r_0 = 1.25$ fm, diffuseness $a = 0.65$ fm, and a spin-orbit component of the same geometry and a depth of 6 MeV.

Inclusion of $2n$ transfer in the calculation is more challenging, the Q value for this reaction favoring high-lying states in ^{67}Cu. The Q-matching condition, together with the fact that no γ rays for transitions in ^{67}Cu were observed, suggests that if the mechanism is conventional transfer only states above the $1n$ separation threshold in ^{67}Cu (9.1 MeV) but below the $2n$ threshold (16.2 MeV) should be considered. Two-step sequential transfer was omitted, as attempting to include it would increase the number of unknowns in the calculation. Because of the lack of information on high-lying states in ^{67}Cu we extrapolated the similarity of the low-lying spectra of ^{65}Cu and ^{67}Cu observed in (p, t) reactions [33] to higher excitation energies. Transfer to states in ^{67}Cu from 10.9 to 14.3 MeV, with spins, parities, and excitation energies of known states in ^{65}Cu [34] was included. A dineutron-like cluster structure for these states with the lowest possible $2n$ angular momentum relative to the ^{65}Cu was assumed. The $2n + {}^{65}$Cu potentials were of Woods-Saxon form, radius $R = 1.25 \times (2^{1/3} + 65^{1/3})$ fm, and diffuseness $a = 0.65$ fm; all spectroscopic factors were set to 1.0. The form factor for the $2n + {}^4$He overlap of ^{6}He was from

Ref. [35]. The optical potential was the same double-folded plus Woods-Saxon combination as in the other channels, with ^{4}He matter density derived from the charge density [36].

Calculated angular distributions for transfer and elastic scattering are shown in Fig. 3. The solid curve in Fig. 3(a) is the sum of the angular distributions for $1n$ transfer to individual states in ^{66}Cu; the agreement with data is good, supporting the assumption that the mechanism is conventional single-neutron stripping to bound states in ^{66}Cu. The $2n$ transfer result, denoted by the dotted line in Fig. 3(a), reproduces well the shape of the angular distribution; the difference in absolute magnitude is not surprising in view of the uncertainties in the $2n$ transfer calculation. These results support the suggestion, prompted by the very large cross section, that the $2n$ transfer is largely the result of a direct, one-step transfer of a dineutron-like cluster.

The effect of transfer couplings on the elastic scattering is shown in Fig. 3(b); the dotted curve denotes the no-coupling calculation and the dashed curve the effect of coupling to $1n$ transfer only. It can be seen that this coupling has a small effect. The solid curve denotes the result of the calculation including both $1n$ and $2n$ transfer couplings. The effect of coupling to the $2n$ transfer channel is much stronger than that of $1n$ transfer, acting to further damp the oscillations and increase the larger angle cross section to better match the data. Although the elastic scattering is still oscillatory compared to the data, a problem usually associated with insufficient absorption, the magnitude is well described. The fusion cross section was calculated using the in-going wave boundary condition. Calculations with no coupling, coupling to $1n$ transfer only, and to both $1n$ and $2n$ transfer give values of 1655, 1631, and 1551 mb, respectively, in good agreement with the measured fusion cross section of 1396(90) mb. The influence of $1n$ transfer coupling on total fusion, like that on the elastic channel, is weak. The relatively good agreement between the measured and calculated values for the various channels in this system seen in Fig. 3 represents an important step towards an understanding of the reaction mechanism for Borromean nuclei at near-barrier energies. Earlier work [15] pointed out the large α particle yield in reactions involving ^{6}He. In particular, the results with a ^{209}Bi target find a ratio of $2n$ to $1n$ transfer cross section of about 2.5–3. For the medium-mass target studied here this ratio is about 10; the difference could be due to the role of target structure.

In summary, exclusive measurements of $1n$ and $2n$ transfer, elastic scattering, and fusion for the Borromean nucleus ^{6}He incident on a medium-mass target at an energy near the Coulomb barrier are reported. The first successful application for a low-energy ISOL beam of triple coincidences between α, neutrons, and γ rays from the targetlike residue and their angular correlations was used to obtain uniquely the $1n$ and $2n$ transfer angular distributions. The present work shows that the main contribution to transfer is due to the $2n$ component, thereby indicating [10] the

dominance of the dineutron structure in ^{6}He. CRC calculations illustrate the important role played by coupling to the two-neutron channel in the reaction mechanism. The availability of low-energy beams of double Borromean ^{8}He, having the highest N/Z ratio, would provide an excellent opportunity to study correlations between the four valence neutrons and to investigate the effect of the continuum in this drip line nucleus.

*Corresponding author.
navin@ganil.fr

[1] M. Dasgupta *et al.*, Annu. Rev. Nucl. Part. Sci. **48**, 401 (1998).
[2] N. Keeley *et al.*, Prog. Part. Nucl. Phys. **59**, 579 (2007).
[3] F. Barranco *et al.*, Eur. Phys. J. A **11**, 385 (2001); E. Vigezzi *et al.*, Nucl. Phys. **A752**, 600 (2005).
[4] Masayuki Matsuo, Phys. Rev. C **73**, 044309 (2006).
[5] M. V. Zhukov *et al.*, Phys. Rep. **231**, 151 (1993).
[6] T. Aumann, Eur. Phys. J. A **26**, 441 (2005).
[7] G. M. Ter-Akopian *et al.*, Phys. Lett. B **426**, 251 (1998).
[8] Yu. Ts. Oganessian *et al.*, Phys. Rev. Lett. **82**, 4996 (1999).
[9] M. Marques *et al.*, Phys. Lett. B **476**, 219 (2000).
[10] L. I. Galanina *et al.*, Phys. At. Nucl. **70**, 283 (2007).
[11] P. Mueller *et al.*, Phys. Rev. Lett. **99**, 252501 (2007).
[12] N. Michel *et al.*, Phys. Rev. C **75**, 031301(R) (2007).
[13] R. K. Adair, Phys. Rev. **111**, 632 (1958).
[14] J. P. Bychowski *et al.*, Phys. Lett. B **596**, 26 (2004).
[15] P. A. DeYoung *et al.*, Phys. Rev. C **71**, 051601(R) (2005).
[16] A. Navin *et al.*, Phys. Rev. C **70**, 044601 (2004).
[17] T. Matsumoto *et al.*, Phys. Rev. C **73**, 051602(R) (2006).
[18] M. Rodriguez-Gallardo *et al.*, Phys. Rev. C **72**, 024007 (2005).
[19] A. M. Moro *et al.*, Phys. Rev. C **75**, 064607 (2007).
[20] J. Simpson *et al.*, Acta. Phys. Hung. New Ser.: Heavy Ion Phys. **11**, 159 (2000).
[21] O. Skeppsted *et al.*, Nucl. Instrum. Methods Phys. Res., Sect. A **421**, 531 (1999).
[22] J. Ljungvall *et al.*, Nucl. Instrum. Methods Phys. Res., Sect. A **528**, 741 (2004).
[23] J. W. Meadows, Phys. Rev. **157**, 1076 (1967).
[24] F. Puhlhofer, Nucl. Phys. **A280**, 267 (1977).
[25] I. J. Thompson, Comput. Phys. Rep. **7**, 167 (1988).
[26] J. J. Kolata *et al.*, Phys. Rev. C **75**, 031302(R) (2007).
[27] G. R. Satchler and W. G. Love, Phys. Rep. **55**, 183 (1979).
[28] J. S. Al-Khalili *et al.*, Phys. Rev. C **54**, 1843 (1996).
[29] T. Neff and H. Feldmeier, Nucl. Phys. **A738**, 357 (2004).
[30] W. W. Daehnick and Y. S. Park, Phys. Rev. **180**, 1062 (1969).
[31] M. R. Bhat, Nuclear Data Sheets **83**, 789 (1998).
[32] O. F. Nemets *et al.*, *Nucleon Clusters in Atomic Nuclei and Many-Nucleon Transfer Reactions* (Ukrainian Academy of Sciences, Kiev, 1988).
[33] J. H. Bjerregaard *et al.*, Nucl. Phys. **85**, 593 (1966).
[34] M. R. Bhat, Nuclear Data Sheets **69**, 209 (1993).
[35] L. Giot *et al.*, Phys. Rev. C **71**, 064311 (2005).
[36] J. S. McCarthy *et al.*, Phys. Rev. C **15**, 1396 (1977).